Modelling the Interfacial Energy of Surfactant-free Amphiphilic Janus Nanoparticles from Phase Inversion in Pickering Emulsions

Dalin Wu,[†] Bernard P. Binks[‡] and Andrei Honciuc[†*]

[†]*Institute of Chemistry and Biotechnology, Zurich University of Applied Sciences, Einsiedlerstrasse 31, 8820 Waedenswil, Switzerland*

[‡]*School of Mathematics and Physical Sciences, University of Hull, Hull HU6 7RX, U.K.*

*Corresponding author: andrei.honciuc@zhaw.ch, tel.:+41-589345283

Submitted to: Langmuir on 5.7.17; revised on: 20.9.17

Includes Supporting Information (SI)

ABSTRACT

Determining the interfacial energy of nanoparticles is very challenging *via* traditional methods that first require measuring the contact angle of several liquids of a sessile drop on pellets or capillary rise in powder beds. In this work we propose an alternative way to model the interfacial energy of nanoparticles directly from emulsion phase inversion data in Pickering emulsions. This could establish itself as a universal and facile way to determine the polarity of nanoparticles relative to a series of standard particles without the need to measure contact angles. Pickering emulsions of several oils in water were generated with a series of snowman-like Janus nanoparticles (JNPs), whose polarity gradually increased with the size of the more polar lobe. Depending on the oil to water ratio and the JNPs lobe size, oil-in-water (o/w) or water-in-oil (w/o) Pickering emulsions were obtained and the affinity of the JNPs to either water or oil can be inferred from the evolution of the emulsion phase inversion curves with these parameters. We further demonstrate that by adopting a simple model for the work of adhesion of JNPs with the water and oil phases, one can quantitatively calculate the relative interfacial energy change of the JNPs with the liquid. In addition, knowledge of the interfacial energy of nanoparticles is useful for employing these in suspension polymerization to create surface nanostructured materials. The o/w and w/o Pickering emulsions obtained from monomers, such as styrene, could be polymerized resulting in colloidosomes or hollow-like materials. The hollow materials exhibited a rather high volume storage capacity for the aqueous phase for extended periods of time, which could be released upon microwaving, making them ideal for use in long-term storage applications of various water-soluble actives.

1. INTRODUCTION

The interfacial energy of nanoparticles (NPs) with a liquid is an important parameter that controls among other functionalities, particle wettability, dispersibility in liquids, granulation,[1] partitioning at interfaces and self-assembly.[2–5] Quantitative determination of the interfacial energy typically first requires measuring the contact angle of several solvents with the surface of interest and subsequently using these values into variants of the Young-Dupré equation[6] *via* models known under different names: OWRK, Fowkes, Wu, *etc*.[7–13] The solvent contact angles on macroscopic surfaces can be trivially determined using the sessile drop method. However, it becomes extremely challenging to use the same measurement techniques for powders in general[1,6] and NPs in particular. Alternatively, different methods have been developed to measure the contact angle on powders none of which is universally applicable or as widely accessible as contact angle goniometry.[1,14] Capillary rise, also known as the Washburn method,[15,16] could be a viable alternative if the powder can be reproducibly packed into the capillary,[17] which in our experience is very challenging to achieve for NPs. Other issues related to determining the interfacial energy of powders were thoroughly debated.[6]

Here we propose an alternative way to evaluate the relative interfacial energy of NPs with liquids without determining the contact angles first, namely from Pickering emulsion phase inversion curves. This method could establish itself as a quick and universal way to estimate the interfacial energy of NPs, for example relative to a known standard, such as a homologous series of Janus nanoparticles (JNPs) with known hydrophilic-lipophilic balance (HLB). We have previously shown that the polarity in a homologous series of JNPs (polystyrene-poly(3-(triethoxysilyl)propyl-methacrylate)) (PS-P(3-TSPM)) increases gradually with an increase in the size of the polar P(3-TSPM) lobe.[18] It is for this reason why the JNPs are especially attractive for future applications, because of the ability to precisely and gradually tune their overall polarity. Their surface energy can be varied by changing the aspect ratio between the lobes of different polarities to the desired conditions without using modifying agents like surfactants.

These JNPs with different polarity lobes are also called ‘solid-state’ amphiphiles and have been proven excellent emulsifiers leading to more stable Pickering emulsions than ones stabilized by homogeneous NPs.[4,19–22,22] In this work we employ a snowman-like series of JNPs with varying surface polarity for the emulsification of various oils and monomers in surfactant-free conditions. Depending on the polarity of the oil, emulsion phase inversion from w/o to o/w takes place at different oil to water ratios (oil: water) across the homologous JNPs series. This allows us to map the phase inversion coordinates and estimate the JNPs-water and JNP-oil interfacial energies. Knowledge of the interfacial energy of NPs is important to predict the type of emulsion but also identify the ideal conditions to carry out a subsequent Pickering emulsion polymerization reaction. Pickering emulsion polymerization can be used for the synthesis of surface nanostructured materials. There have been many reports on o/w Pickering emulsion polymerization stabilized by homogeneous NPs and JNPs,[23–26] but significantly less reports on w/o Pickering emulsion polymerization in surfactant-free conditions.[27] This is partly due to the

difficulty in obtaining NPs sufficiently hydrophobic and yet dispersible enough to form a stable colloid in water. JNPs offer more flexibility because one side of the particle can be kept very hydrophobic whereas the polar side provides good stability and dispersibility in water. The polarity balance can be tuned to match the polarity of the oil. The JNPs were able to fulfill a dual role, first as emulsifiers and stabilizers of monomer oil droplets in water and secondly as surface nano-structuring agents bearing different chemical functionalities for the solid materials obtained.[28,29] Here, both polystyrene (PS) colloidosome-like structures and polystyrene hollow structures resembling Swiss cheese with closed cavities could be obtained from styrene-in-water and water-in-styrene Pickering emulsions stabilized by JNPs *via* suspension polymerization. The hollow polystyrene material is filled with the water phase from the original w/o emulsion. Water could be released from the hollow structure by microwaving and this could find application in long-term storage of actives, such as proteins, dyes, pharmacological or antimicrobial agents.

2. EXPERIMENTAL

Materials: Styrene (Sty) (> 99%), divinylbenzene (DVB) (80%), sodium 4-vinylbenzenesulfonate (NaVBS) (> 90%), ammonium peroxydisulfate (APS), methanol (> 99.9%), ethanol (> 99%), heptane (99.9%), methyl methacrylate (MMA) (> 99%), toluene (Tol) (> 99%), dichloromethane (DCM) (>99%), ammonium hydroxide solution ($NH_3.H_2O$) (28%), 3-(triethoxysilyl)propyl-methacrylate (3-TSPM) (>99%) and aluminum oxide (Al_2O_3 basic) (≥ 98%) were purchased from Sigma-Aldrich. Sty and DVB were passed through Al_2O_3 to remove the stabilizer before usage. Azo-bisisobutyronitrile (AIBN) was purified by re-crystallization twice from methanol and stored at -20 °C before use. Other reagents were used as received. Ultrapure water (UPW; resistivity at 298 K = 18.2 MΩ cm) was obtained from an Arium 611 VF water purification system (Startorius Stedim Biotech, France) and was used as the aqueous phase in all experiments.

Nanoparticle synthesis and characterization: The PS (non-polar lobe) seed NPs and JNPs with different 3-TSPM (polar lobe) lobe sizes were synthesized according to the procedures previously reported.[18] They were characterized using scanning electron microscopy (SEM) (FEI Quanta FEG 250), operating at an accelerating voltage of 5–30 kV in the secondary electron mode in high vacuum mode (3×10^{-6} – 1.8×10^{-5} mbar).

Pickering emulsion preparation and characterization: All the emulsions were prepared for a total volume of oil and water of 9 mL. The concentration of particles, regardless of the oil: water volume ratio, was 2.22 mg/mL. The oil also contained 0.01 wt.% of hydrophobic Hostasol Yellow 3G dye. The mixture of oil, water and JNPs was homogenized using a Branson 450D sonifier with a ½ inch processing tip with an intensity amplitude of 70% for 30 s at room temperature to form Pickering emulsions. The emulsions were characterized using an inverted fluorescence microscope (IX51, Olympus, Tokyo, Japan) with a 100 W mercury discharge burner (lamp: USH-103OL, Ushio, Tokyo Japan), 460 nm - 495 nm excitation filter and CPLN-PH 10X microscope objective lens. The lipophilic dye partitions into the oil phase exclusively and thus the emulsion type was

determined to be w/o if the droplets (dispersed phase) appeared dark in the fluorescence image and o/w if the dispersed phase appeared bright.

Measurement of oil-water interfacial tension: The surface and interfacial tension (IFT) measurements were carried out through the evaluation of the equilibrium drop shape using a DataPhysics OCA 15Pro contact angle goniometer equipped with an automatic dosing system. The IFT was measured by analyzing the contour of a pendant drop of oil within water. The images of the drop shape were captured in real time and then digitally analyzed using edge-detecting DataPhysics SCA 22 software module by fitting the contour of the droplet to the Young-Laplace equation. The same procedure was followed for measuring the surface tension (ST) of the pure liquids in air. For methyl methacrylate, styrene, toluene and heptane, the droplets were generated at the apex of an upward-bended dosing needle within an aqueous phase contained in a 20 cm cubic quartz cuvette. For dichloromethane, the droplet was generated at the apex of straight dosing needle with an aqueous phase contained in a 20 cm cubic quartz cuvette at 21 °C.

Polymerization of o/w Pickering emulsion stabilized by (4 mL 3-TSPM) JNPs: The o/w emulsion was prepared by mixing 5 mL aqueous dispersion of JNPs (4 mL 3-TSPM), c = 5 mg/mL, with 4 mL styrene containing 40 mg of AIBN initiator. The mixture was homogenized using a Branson 450D sonifier with a ½ inch processing tip with an amplitude of 70% for 30 s with ice cooling to form a stable o/w Pickering emulsion. The ice cooling is necessary to avoid activation of the radical initiator. After removal, if any, of the non-emulsified styrene, the emulsion was polymerized overnight at 70 °C without stirring. The solidified PS Pickering emulsion was further purified by washing with methanol before characterization by SEM. The polymerized Pickering emulsions were sputtered with Au with a sputter-coater (Q15OR-S Sputter Coater, Quorum) at 20 mA for 30 sec under an Ar atmosphere (pressure: 5×10^{-2} mbar). Then the surface structures were characterized by low vacuum SEM with 5.0 kV under 0.40 mbar.

Polymerization of w/o Pickering emulsion stabilized by (2 mL 3-TSPM) JNPs: The w/o emulsion was prepared by mixing 4 mL aqueous dispersion of JNPs (2 mL 3-TSPM), c = 5 mg/mL, with 5 mL styrene containing 50 mg of AIBN initiator. The mixture was homogenized using a Branson 450D sonifier with a ½ inch processing tip with an amplitude of 70% for 30 s with ice cooling to form a stable w/o Pickering emulsion. Next the w/o emulsion was polymerized overnight at 70 °C without stirring. The solidified w/o Pickering emulsion was crushed into small pieces and further purified by washing with methanol before characterization by SEM. Prior to SEM analysis the solidified w/o emulsion was treated in a similar fashion to the o/w solidified Pickering emulsion.

3. RESULTS AND DISCUSSION

3.1. Homologous series of JNPs

The surfactant-free polymeric JNPs were synthesized according to a procedure previously reported,[18] but from 22% smaller starting seed PS NPs. The seed PS NPs had a diameter of 141 ± 11 nm, which were then used to grow a second lobe by seeded emulsion polymerization of 3-TSPM and phase separation between PS and P(3-TSPM) happened in the presence of APS radical initiator. By changing the volume of 3-TSPM monomer to the mass of the starting PS seed NPs, typically using 0.5, 1, 2, 3 and 4 mL per 1 gram of starting PS seed NPs, a homologous series of five types of JNPs with varying P(3-TSPM) lobe size were obtained (Table S1). The resulting JNPs are depicted in the SEM images in Figure S2 and the notation we adopt to differentiate between the members of the series is (0.5 mL 3-TSPM) JNPs for the smallest 3-TSPM lobe JNPs and (4 mL 3-TSPM) for the largest 3-TSPM lobe JNPs . The series of JNPs with varying lobe sizes bears resemblance to a homologous series of molecular surfactants, for example linear alkyl sulfonate or fatty acids, whose polar functional group remains the same while the non-polar alkyl chain increases in the series. The size of the JNPs lobes and their corresponding aspect ratio is given in Table S1 & S2. The HLB parameter is often used to gauge *a priori* the 'amphiphilicity' of a surfactant in a homologous series. Therefore we have also calculated this for the homologous series of the JNPs used here, according to the procedure already described,[18] and the results are summarized in Table S2. It can be observed that the obtained HLB values span the entire range of the HLB scale (Griffin's classification).[30,31] Typically an HLB << 10, *e.g.* $HLB_{(0.5\ mL\ 3\text{-}TSPM)\ JNP}$ = 5, indicates a good w/o emulsifier with a higher affinity for oil and an HLB >> 10 indicates a good o/w emulsifier with a higher affinity for water, *e.g.* $HLB_{(4\ mL\ 3\text{-}TSPM)\ JNP}$ = 16.

3.2. Effects of oil type on Pickering emulsions stabilized by JNPs

The homologous series of JNPs and the PS seed NPs were used in the emulsification of solvents and monomers with different polarities with water, starting from the most polar to the least polar: MMA, DCM, Sty, Tol and Hep. The polarity of the solvents was ranked according to the fraction of the dispersive component relative to the total Hansen parameter,[32] given in Table S3. The emulsification of the mentioned oils was performed at different oil: water ratios at fixed overall particle concentration of 2.22 mg/mL. Depending on their polarity, the oils have different solubility in water also given in Table S3. The emulsification results for Sty and water are represented as formulation-composition maps showing images of the emulsions and fluorescence microscopy snapshots of the droplets formed in Figure 1A, and the corresponding emulsification vials photographed under UV light in Figure 1B. The emulsification results for the other solvents are presented in Figures S3-S6. The formulation-composition maps relate the type of Pickering emulsion obtained with the oil: water ratio and the P(3-TSPM) lobe size of the JNPs. In these maps, catastrophic emulsion phase inversion from w/o to o/w is depicted by the

vertical arrow (decreasing oil: water ratio) and static transitional emulsion phase inversion from w/o to o/w by the horizontal arrow (increasing P(3-TSPM) lobe size). It is important to note that at fixed oil: water ratio, transitional phase inversion from w/o to o/w may only be induced by increasing the polarity of the particles, according to the rules of Finkle *et al*. and Bancroft,[33,34] which in this case is due to increase in the size of the P(3-TSPM) lobe of the JNPs.

The Pickering emulsions, regardless of the oil, at extreme oil:water volume ratios such as 1 : 8 and below or above 8 : 1 are not stable exhibiting complete coalescence within 12-48 h. For mid-range oil : water volume ratios, especially near that required for phase inversion, the emulsions proved to be extremely stable to coalescence regardless of the oil for at least six months of observation time. Creaming or settling down of o/w or w/o emulsions was observed however in all cases, due to difference in density of oil and water. Qualitatively, it can be observed that there is an effective increase in the average o/w and w/o emulsion droplet size upon increasing the JNPs' P(3-TSPM) lobe size, *i.e*. from left to right in Figures 1A, S3, S4, S5 and S6. Also it can be observed that the larger emulsion droplets may be elongated due to shearing during their formation and were covered with the Janus particles before they could relax to a spherical shape.

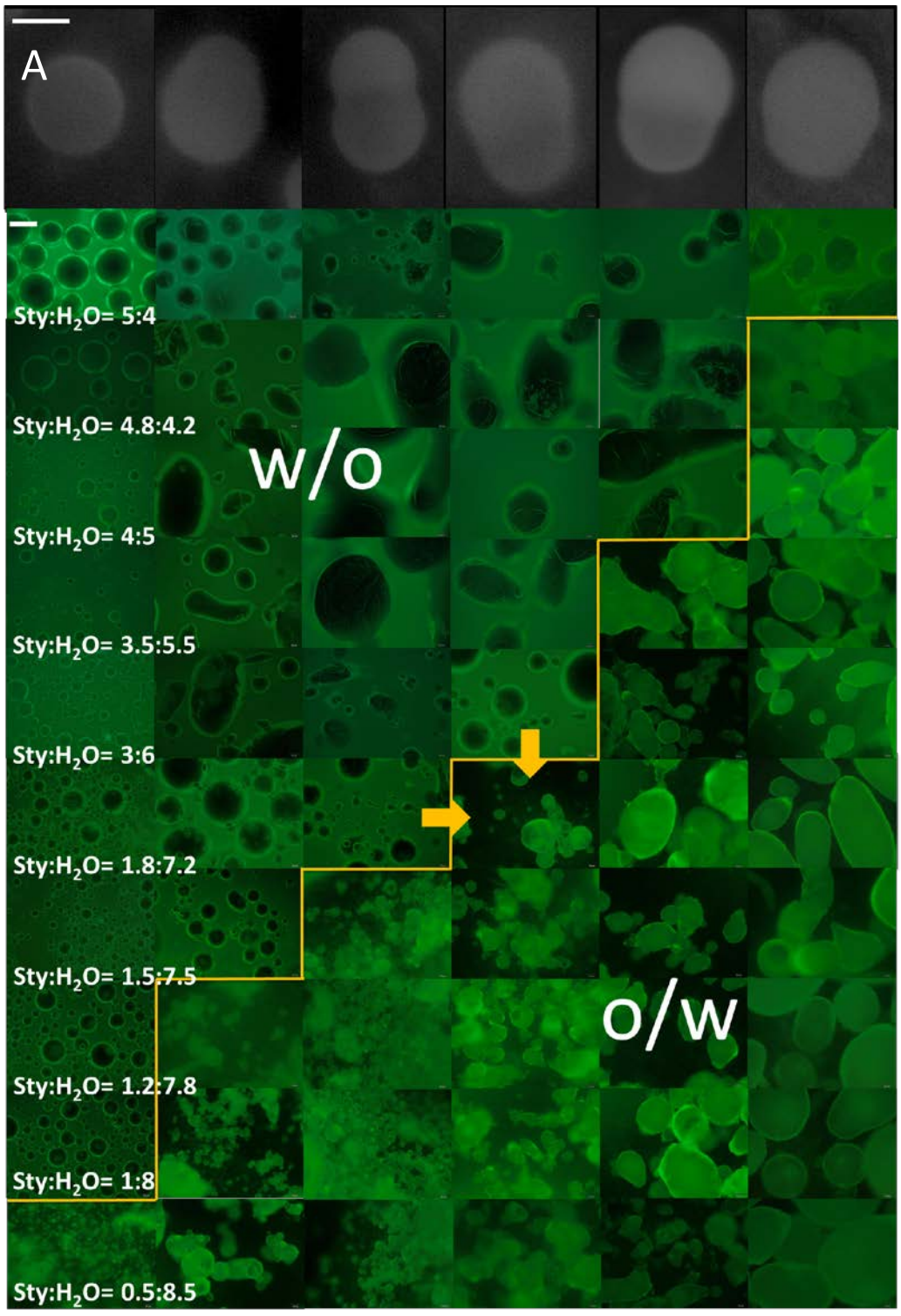
A
Sty:H2O= 5:4
Sty:H2O= 4.8:4.2
w/o
Sty:H2O= 4:5
Sty:H2O= 3.5:5.5
Sty:H2O= 3:6
Sty:H2O= 1.8:7.2
Sty:H2O= 1.5:7.5
o/w
Sty:H2O= 1.2:7.8
Sty:H2O= 1:8
Sty:H2O= 0.5:8.5

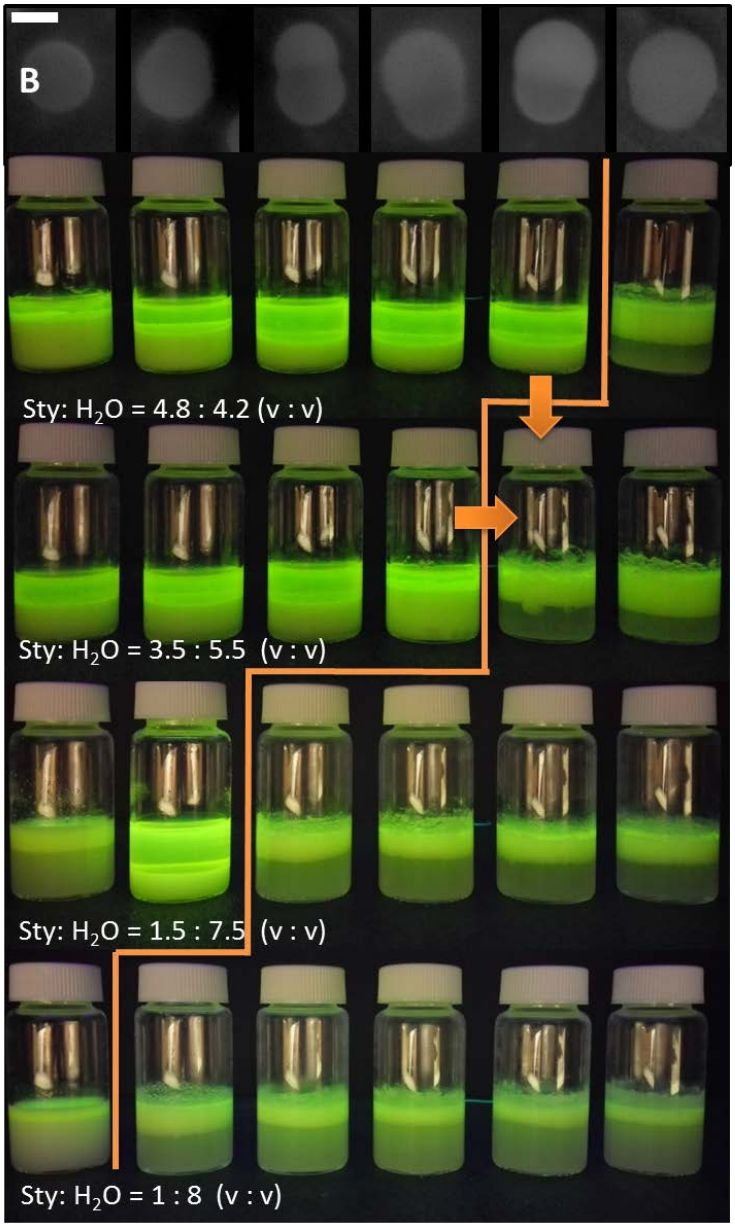

Figure 1. (A) Formulation–composition maps with corresponding fluorescence microscopy images (scale bar = 200 µm) for the emulsions obtained from styrene and water with the homologous series of JNPs. The top row depicts PS seed nanoparticles and five JNPs with increasing P(3-TSPM) lobe size (scale bar = 100 nm), while the subsequent rows represent a different volume ratio of styrene to water (given). The six columns represent emulsions conferred by each type of NP. The yellow line indicates the boundary between w/o (left) and o/w (right) emulsions; the vertical arrow indicates catastrophic phase inversion and the horizontal arrow "static" transitional phase inversion. (B) Photographs of the emulsification vessel under UV-light showing the types of emulsions obtained for the corresponding JNP (scale bar = 100 nm). The photos were taken immediately after emulsion formation. Emulsion phase inversion is also indicated by arrows. For reasons of space, images are restricted to four oil:water ratios.

Representing the set of data for all oils differently, Figure 2 shows the influence of both the lobe size and the oil volume fraction on the type of emulsion formed. Below each curve, only o/w emulsions are found while

above each curve only w/o emulsions are formed and it can be clearly observed that the phase boundary lines shift as a function of the lobe size of the JNPs and the oil polarity (Table S3), also depicted in Figure S8. The smallest volume step near the boundary line for which we were able to prescisely establish the emulsion type *via* fluorescence microscopy was 0.2 mL, which corresponds to a oil volume fraction ϕ_o of 0.02.

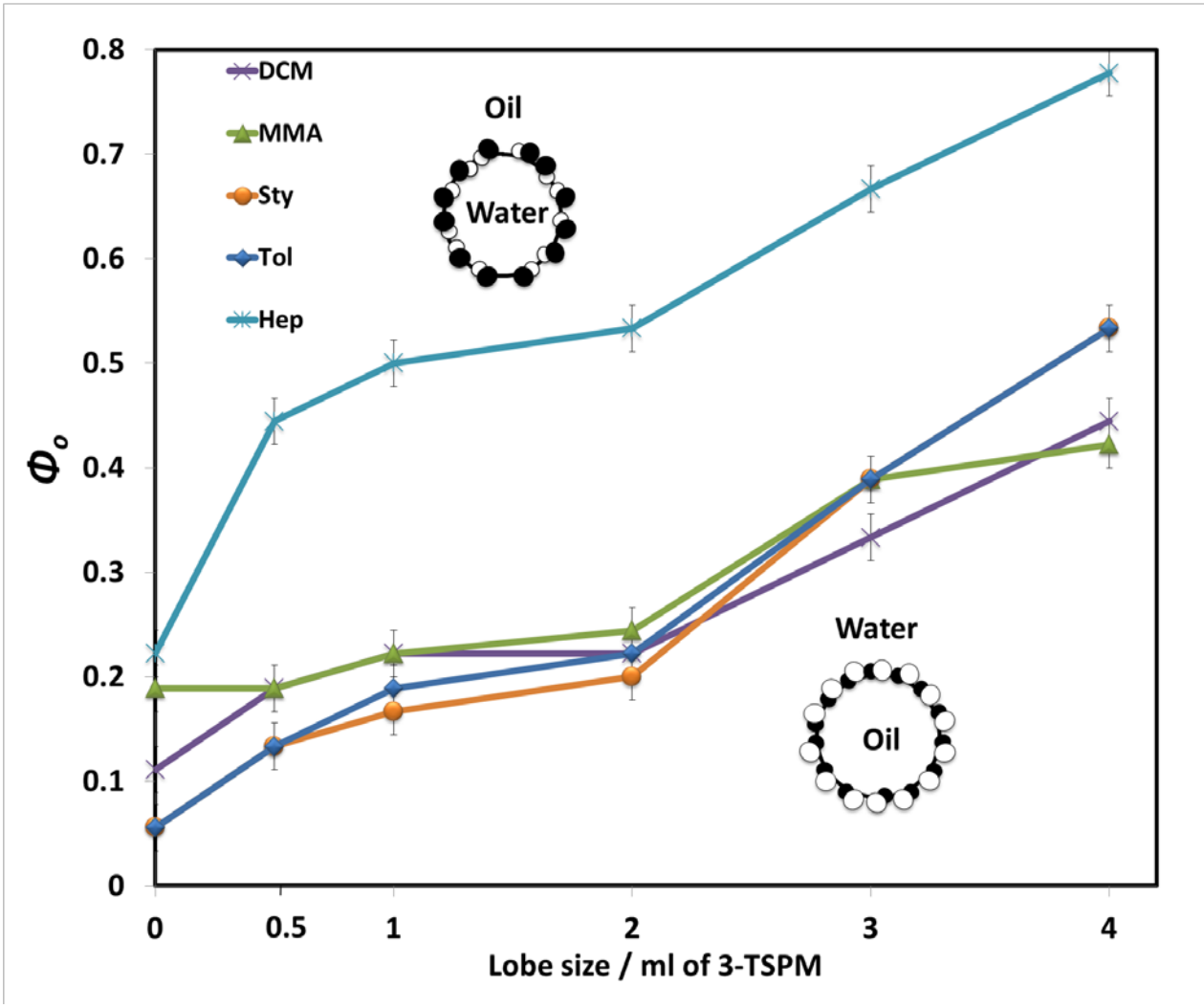

Figure 2. Summary of emulsification results obtained for the PS seed nanoparticles and the homologous series of JNPs with different oils: DCM, MMA, Sty, Tol and Hep. The curves represent the boundary between the different types of emulsion with o/w below the curves and w/o above them. The y-axis is the oil volume fraction in each emulsion, $\phi_o = V_{oil}/(V_{oil}+V_{water})$. The overall concentration of the JNPs was 2.22 mg/mL. The cartoon insets depict the curving of the interface towards oil and towards water. The vertical error bars correspond to the smallest volume fraction step for which the emulsion type could be reliably determined.

Qualitatively, some general trends can be observed from Figure 2. For smaller lobe JNPs, *e.g.* (0.5 mL 3-TSPM), catastrophic phase inversion occurs at smaller values of ϕ_o than for the larger lobe ones, *e.g.* (4 mL 3-TSPM). This suggests that the adhesion of the former JNPs to the oil is stronger, in other words they are able to 'curve'

the interface towards water even for ϕ_o values smaller than say 0.3. Further, with the exception of heptane, catastrophic phase inversion for PS seed nanoparticles and 0.5 mL 3-TSPM JNPs occurs at larger ϕ_o values upon increasing the solvent polarity, from Tol to MMA, suggesting that the affinity for the more polar oil phase decreases. By contrast, for bigger lobe JNPs (4 mL 3-TSPM), catastrophic phase inversion occurs at lower ϕ_o when the polarity of the oil increases clearly due to their increased affinity towards the more polar oils, see Figure S8 & Table S3; this trend obtained for the (4 mL 3-TSPM) JNPs as a function of the oil polarity is the same as that reported by Binks and Lumsdon[35] for homogeneously coated silica nanoparticles of intermediate hydrophobicity. For the JNPs with intermediate lobe sizes, catastrophic phase inversion varies in a complex way with oil polarity, and appears as a convolution between the two extreme situations described above. In addition the Hep's curve can be seen as a special case, Figure 2, and the reason for this is that heptane is a purely dispersive liquid. The work of adhesion with the particle surface is limited only to dispersive interactions, which explains the lowest adhesion of the particles to heptane observed compared to any other oil, *i.e*. largest ϕ_o.

Clearly, the position of the inversion boundary separating the different emulsion types is given by the balance that exists between the adhesion forces of the particle with water compared with that of the particle with oil. For example, if the particle has a higher affinity for the water phase than the oil phase, o/w emulsions are obtained by curving the oil-water interface such that it becomes concave on the oil side. If the particle affinity for the two phases is reversed, w/o emulsions are preferred with opposite curvature of the oil-water interface. This is sketched in Figure S7. Obviously, in the absence of any particles, no emulsions would be obtained.

3.3. Model for calculating particle-solvent relative interfacial energies from emulsification data

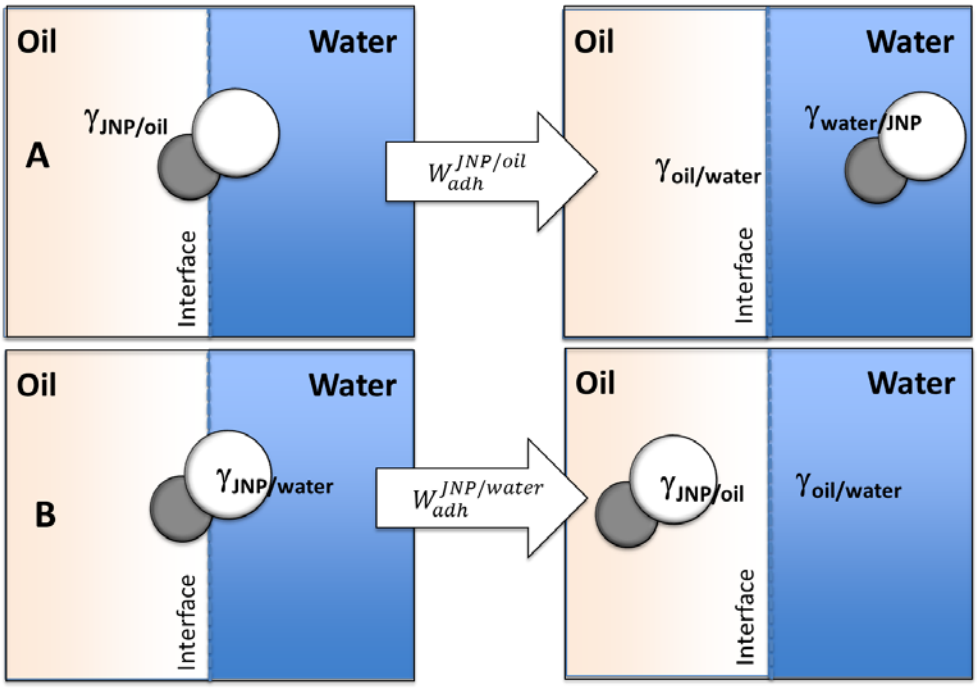

Figure 3. Cartoons depicting the graphical interpretation of Dupre's formalism for the work of adhesion of (A) JNP to oil and (B) JNP to water, with the initial state of the particle at the interface without a preferential orientation (left) and the final state of the particle completely immersed in either of the bulk phases (right).

Next, we propose a model to extract quantitative information such as the interfacial energy of the particle-solvent interaction from the emulsion phase inversion curves by equating the work of adhesion at each point on these curves in Figure 3. In order to translate the qualitative information from the emulsion phase diagram into equations, we start by considering that: (*i*) each point lying on the phase boundary curve is a point of equal probability for the formation of o/w or w/o emulsions; (*ii*) the volume ratio of oil:water, henceforth labeled as f, at which the o/w to w/o transition occurs is a function of the polarity of the particle and of the solvent, see Figure S8, and is the key parameter that will be included in the model. Namely, we assume that if the position of the emulsion phase boundary function described by the f is lower than unity then the JNPs prefer the oil phase and if higher than unity then the JNPs prefer the water phase and (*iii*) at the emulsion phase boundary the work of adhesion or "spreading pressure"[36] of the oil to JNPs can be related to that of water with the parameter f. Conceptually, this work of adhesion could in principle also be related to the adhesion force between the topmost layer of the JNPs with the molecules of the liquid from the second phase, see Figure S7 and the discussion thereafter in SI.

Next, we attempt to relate the work of adhesion of the JNPs to oil $W_{adh}^{JNP/oil}$ (mJ/m^2) with that to water $W_{adh}^{JNP/water}$ with the help of the parameter f which contains information of the JNPs' affinity to the liquids. The

resulting empirical relationship must reflect the trends observed in Figure 2, as a function of changing oil polarity and particle surface polarity. In order to do that we follow the evolution of the emulsion phase boundary function of two independent parameters: (*A*) same JNPs but different oils and (*B*) same oil but different JNPs.

(A) For the same particle type but different oil, f and ϕ_o changes with the polarity of the oil. The polarity of the oils was estimated from the fraction of the polar component of the corresponding Hansen parameters and ranked accordingly in Table S3. At each value of *f*, for a given JNP, the relative affinity of the JNPs to either phase can be related by:

$$\boldsymbol{W_{adh}^{JNP/oil} = \frac{1}{f} \cdot W_{adh}^{JNP/water}} \quad (1)$$

where $W_{adh}^{JNP/oil}$ is the work of adhesion of oil to the JNP and $W_{adh}^{JNP/water}$ is the work of adhesion of water to the JNP. By relating the work of adhesion of the JNP to each of the phases with the help of the parameter *f* in Equation 1 we attempt to account how much stronger the particle surface is wetted by one of the liquids compared with the other. The better spreading of oil or water on the JNP surface in Figure 3 should be interpreted by the immersion depth of the JNP in one of the phases. Equation 1 enables us to gauge this interaction strength, that is how much stronger or weaker is the adhesion of the JNP to oil than that to water by the factor 1/*f*. Therefore, based on the experimental observations in Figure 2, we have placed *f* in the denominator in Equation 1. The experimental observations tell us that when w/o emulsions are observed at very low ϕ_o, then $1/f > 1$. Hence, the adhesion of oil to the JNP is stronger than that of water to the JNP and the oil-water interface remains concave on the water side even for very low *f* values, see Figure S7A. The reason why the volume ratio *f* instead of the volume fraction ϕ_o was used in Equation 1 is that 1/*f* is a more convenient factor and readily understood intuitively when it becomes larger or smaller than unity. Further, Equation 1 can be re-written in an equivalent form:

$$\boldsymbol{\gamma_{oil/water} + \gamma_{JNP/water} - \gamma_{JNP/oil} = \frac{1}{f} \cdot W_{adh}^{JNP/water}} \quad (2)$$

where $\gamma_{oil/water}$ is the IFT of the oil-water interface (mN/m also expressed as mJ/m^2), $\gamma_{JNP/water}$ is the interfacial energy of the JNP/water interface (mJ/m^2) and $\gamma_{JNP/oil}$ and $\gamma_{JNP/water}$ are the interfacial energies of the JNP-oil and JNP-water interfaces respectively. Here we note that the units of the work of adhesion, the energy per unit area, are the same as the interfacial energy (for solid/liquid interfaces) and interfacial tension (for liquid/liquid interfaces) and the latter two are very often used interchangeably.. It is important to note that for the left-hand side of Equation 2 we have applied Dupré's formalism for the work of adhesion considering the JNP/oil as the initial state and the energy of the two newly formed interfaces JNP/water and oil/water as the final state.[36] Note that because particles are already present at the interface we consider for the initial state that the oil-water interface is pinned at the particle surface, see Figures 3A and B. For a better understanding, this situation is depicted in the cartoon in Figure 3A, which is the graphical representation of the Dupré's formalism for the

work of adhesion of JNP/oil, $W_{adh}^{JNP/oil}$, as defined above. Here, there is no need to assume a preferential orientation of the JNPs at the interface. Therefore we have depicted the particle lying flat on its long axis but the orientation could be random. It is now clear that if there is a larger affinity of the JNPs to water (let's say if the polarity of the oil decreases) and the particle is rather polar (compare *f* and ϕ_o for MMA to Tol in Figure 2) for the (4mL 3-TSPM) JNPs), the work of adhesion of the JNPs to oil must be relatively smaller and thus the values of *f* and ϕ_o at which the o/w to w/o transition occurs are larger. The critical point of this model is that Equation 1 sets a relative gauge as to how much smaller $W_{adh}^{JNP/oil}$ is than $W_{adh}^{JNP/water}$ as a function of the observed experimental value *f*. It is now instructive to emphasize that the variable *f*, which is the ratio of oil:water that we determined experimentally, is a good relative (not absolute) indicator for the particle affinity to either of the oil or water phases. If $f = 1$, then the oil and water volumes are equal and the affinity of the particles to either of the phases is relatively equal. For any value of $f < 1$, $\phi_o < 0.5$, the affinity of the particles to oil is larger (or $1/f$ times larger) and conversely for any $f > 1$ and $\phi_o > 0.5$ the affinity of the particle to water is larger (f times larger). Finally, the affinity of the JNPs to either phase is estimated in our model by the work of adhesion, see Equation 1.

(B) For the same oil but different particle type, *f* and ϕ_o increase with the increase in the lobe size of the JNPs,[18] as can be seen from Figure 2. All the emulsion inversion boundaries have a positive slope meaning that the adhesion of (4 mL 3-TSPM) JNP to oil should be less than that of (0.5 mL 3-TSPM) JNP when *f* increases. It is therefore clear that *f* contains information on the JNPs affinity to either liquid in both emulsion phases. Thus, the work of adhesion to the oil must decrease with increasing *f* , ϕ_o and increasing particle polarity. In order to translate this qualitative trend into equations, namely *f* increases when the JNPs' polarity increases, we modify the left-hand side of the Equation 2 so that the work of adhesion of the JNPs to the oil, $W_{adh}^{JNP/oil}$ decreases with an increase in the particle polarity. The $W_{adh}^{JNP/oil}$ decreases when we allow $\gamma_{JNP/water}$ to decrease; one can do this by either multiplying the latter term with *1/f* or multiplying the $\gamma_{JNP/oil}$ by *f*. Allowing $\gamma_{JNP/water}$ term to decrease by the factor *1/f* is perfectly justified considering that a higher affinity of water to the increasingly polar particle's surface is always indicated by a lower interfacial tension. Therefore we relate the interfacial tension of the different JNPs to water, $\gamma_{JNP/water}$, inversely with *f* and modify Equation 2 to include this effect:

$$\boldsymbol{\gamma_{oil/water} + \frac{1}{f} \cdot \gamma_{JNP/water} - \gamma_{JNP/oil} = \frac{1}{f} \cdot W_{adh}^{JNP/water}} \qquad (3)$$

As can be seen the way we have modified the left-hand side of the above equation in order to allow $W_{adh}^{JNP/oil}$ to decrease by introducing the *1/f* factor is not unique. In fact this can be done in three different but equivalent ways (multiplying only $\gamma_{JNP/water}$ by *1/f*, multiplying $\gamma_{JNP/oil}$ by *f*, or both) as long as the overall $W_{adh}^{JNP/oil}$ is allowed to decrease with increasing particle polarity. For simplicity we considered only one of these

possibilities. Expanding the $W_{adh}^{JNP/water}$ term in Equation 3, we can now write the final expression for a given particle and given oil as:

$$\boldsymbol{\gamma_{oil/water} + \frac{1}{f} \cdot \gamma_{JNP/water} - \gamma_{JNP/oil} = \frac{1}{f} \cdot (\gamma_{oil/water} + \gamma_{JNP/oil} - \gamma_{JNP/water})} \qquad (4)$$

Again we note that for the right-hand side of Equation 4 we have applied Dupré's formalism for the work of adhesion considering the JNP/water as the initial state and the energy of the two newly formed interfaces JNP-oil and oil-water as the final state. In other words, $W_{adh}^{JNP/water}$ is the energy needed to detach the particle from the water surface and transfer it into the oil phase. Similar to the earlier exposition, Figure 3B shows the graphical representation of the Dupré's formalism for the $W_{adh}^{JNP/water}$ and accordingly the right-hand side of Equation 4 is the expansion of the right hand term of Equation 1. As already explained, the multiplication with *1/f* of the right-hand side is to reflect the change in $W_{adh}^{JNP/oil}$ when the JNP changes. In other words we see that *f* becomes increasingly larger with an increase in the polarity of the JNPs, Figure 2, signaling that the adhesion of the JNPs to the water phase has increased, therefore, $W_{adh}^{JNP/water}$ has increased with a factor of *f*. Upon re-arrangement, the last expression becomes:

$$\boldsymbol{(f-1)\gamma_{oil/water} = (f+1)\gamma_{JNP/oil} - 2\gamma_{JNP/water}} \qquad (5)$$

Finally, we have now arrived at an explicit form that directly relates the oil-water interfacial energy with the difference in interfacial energies of the JNP with oil and the JNP with water. From Equation 5 we can observe that when catastrophic phase inversion discussed above occurs at an oil:water ratio $f > 1$, then $\gamma_{JNP/oil} > \gamma_{JNP/water}$ and when it occurs at an oil:water ratio $f < 1$, then $\gamma_{JNP/oil} < \gamma_{JNP/water}$, where $f = 1$ corresponds to $\phi_o = 0.5$ in Figure 2. With the help of Equation 5 we can evaluate the interfacial energies by creating a linear system of equations consisting of five equations corresponding to each of the five oils having six unknowns being five $\gamma_{JNP/oil}$ interfacial energies plus the $\gamma_{JNP/water}$ interfacial energy. The system of equations was solved for each of the JNPs and the seed PS nanoparticles using the Linear Simplex algorithm in the Solver package of Excel. A global minimum was identified and the results are summarized in Table S4 and the change in interfacial energy of the solvents with the JNP lobe size is also given in Figure 4. Here we note that for particles with non-smooth surface morphologies, the obtained interfacial energies can be regarded as effective or coarse-grained. From these curves, it can be observed that the interfacial energy of the JNPs with water and the more polar solvents DCM and MMA decrease with the increase in the size of the P(3-TSPM) lobe. This means that the overall polarity of the JNPs increases with the increase in the lobe size. The second observation is that a decrease in the interfacial energy suggests a large work of adhesion as discussed above, *i.e.* a better affinity of the liquid to the JNP surface. On the other hand, the least polar solvents such as Hep and Tol show an increase in interfacial energy with an increase in the lobe size, suggesting that the work of adhesion with the JNPs decreases. However, the most dramatic increase in interfacial energy is for the case of Hep, which is rather

expected considering that linear alkanes can only interact *via* dispersion forces. For the case of Sty solvent, its interfacial energy with the JNPs evolves as intermediate between the most polar and the least polar solvents. Interestingly, the predicted magnitude of the JNP/oil interfacial energies appears to decrease with increasing polarity of the oil MMA > DCM > Sty > Tol, comparable to the solvent polarity ranking in Table S3. Furthermore, a low interfacial energy such as that observed for Tol indicates a good adhesion and wettability to particles and also that the JNPs might be well dispersible in such a solvent.

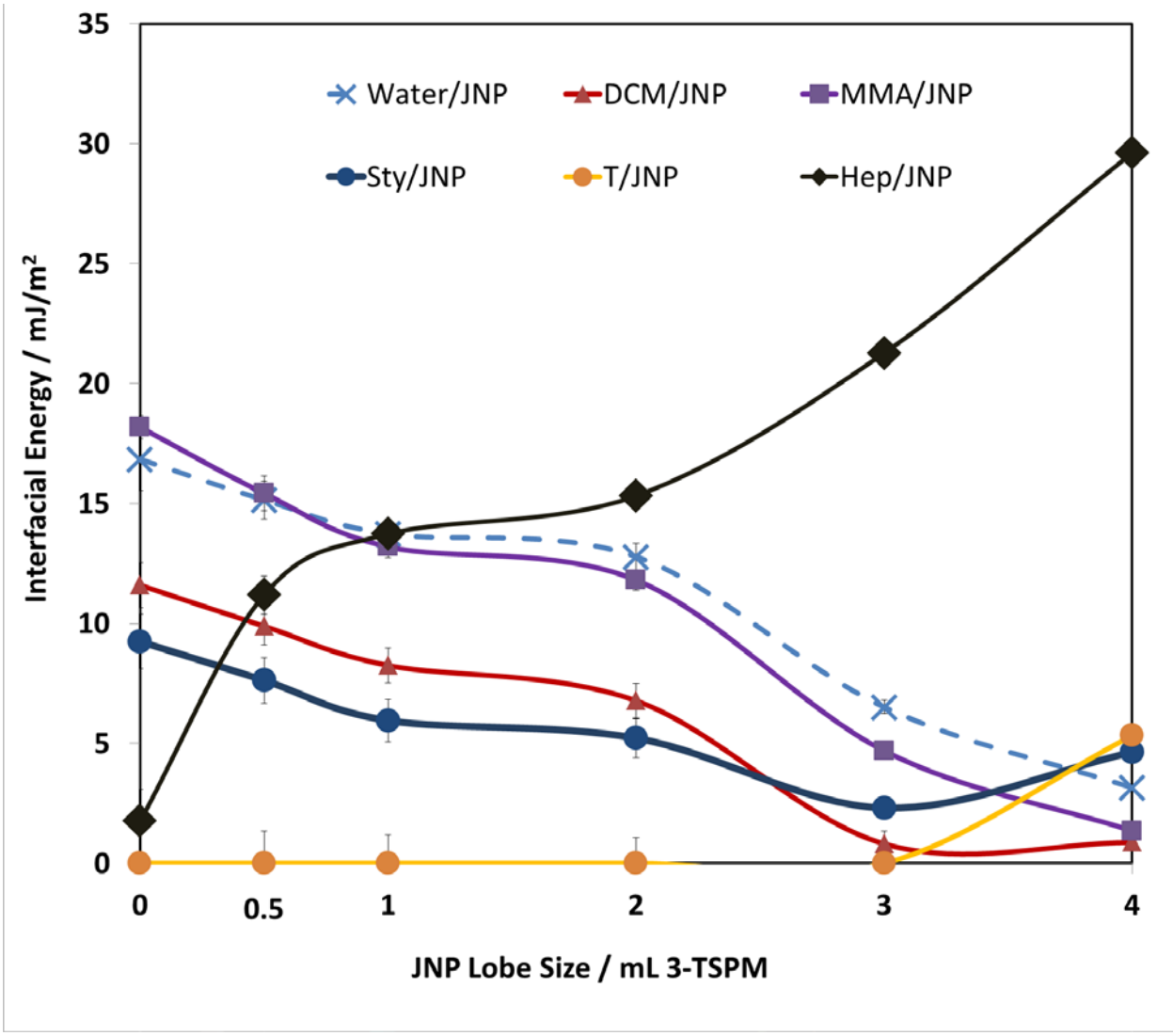

Figure 4. Evolution of the interfacial energies of JNP/water and JNP/oil *versus* lobe size for different oils; the lobe size "0" mL 3-TSPM refers to the PS seed particles. The increase in polarity of the JNPs with the P(3-TSPM) lobe size can be spotted from the relative strong decrease in the JNP/water interfacial tension. The error bars associated with the interfacial energies of JNP/water and JNP/oil correspond to the standard deviation obtained by propagating the errors of *f* in the corresponding system of equations using Equation 5.

Applying the simple model described in Equation 5, we are able to calculate the relative interfacial energies of the JNPs with the different oils. Furthermore, we also attempted to calculate the surface energy of the JNPs by solving the appropriate system of equations that take into account the dispersive and polar components to the surface energy:[11]

$$\gamma_{oil/JNP} = \gamma_{oil} + \gamma_{JNP} - 2 \cdot \sqrt{\gamma_{oil}(p)} \cdot \sqrt{\gamma_{JNP}(p)} - 2 \cdot \sqrt{\gamma_{oil}(d)} \cdot \sqrt{\gamma_{JNP}(d)} \quad (6)$$

but no unique solution could be found. We can now conclude that the model we have presented can be very useful to predict the relative interfacial energies of particles with oils and water based on catastrophic and transitional phase inversion boundaries derived from emulsion data.

In summary, the interfacial energy values of the JNPs with the liquids obtained from the above model are not absolute but relative and depend on several assumptions: (1) at the emulsion phase boundary the work of adhesion or "spreading pressure" of the oil to JNPs can be related to that of water with the parameter *f*; (2) that the 1/*f* factor can be used to gauge the interaction strength by the relative affinity of the JNPs to either of water or oil phases. Although this may seem an arbitrary choice, it is the only way to translate the qualitative information from the emulsion phase diagram into interfacial energies, because the position of the emulsion phase boundary (*f*) is the only parameter containing information of the particle's relative affinity to either oil or water phases. The main limitation of this model is that instead of *f* one can choose the volume fraction ϕ_o, the mole fraction, *etc*. and it is for this reason that one could only expect relative information for the interfacial energies. If *f* could be fixed by other means such as experimental determination of the interfacial energy then establishing the appropriate scaling factor, one could expect absolute results. We have attempted this but unfortunately we could not reliably measure the interfacial tension of the JNPs by classical methods, which rely first on determining the contact angle *via* goniometry or Washburn methods. Such difficulties in measuring the contact angle on nanoparticles emphasize in fact the necessity for an alternative way to evaluate the interfacial energies. While the model proposed here suffers from the above assumptions it is nevertheless the first attempt in this direction. Alternatively, due to lack of measurement options, researchers are forced to assume that the contact angle of a fluid on polymeric nanoparticles is the same as that on flat surfaces of the same material on which they can easily measure the contact angle, but unfortunately these assumptions may lead to erroneous results since the surface of the polymeric particles obtained by emulsion polymerization is strongly influenced by the type and nature of the initiator used as we have shown previously. Therefore, our model of determining the interfacial energies could be used on any particles with unknown polarity and compared to the standard scale used here.

3.4. Pickering emulsion polymerization

Molecular surfactants are commonly employed in emulsion polymerization. The classical radical emulsion polymerization is a standard way for generating nanoparticles from a variety of monomers, including styrene and

MMA.[37] The mechanism of emulsion polymerization is well understood and typically proceeds with homogeneous nucleation and growth of the polymeric particles *via* a surfactant micelle-mediated mechanism.[37,38] The emulsion droplets act as a reservoir of monomer whose molecules migrate through the aqueous phase and support the growth of the polymer particles until completely exhausted. Particles can be successfully employed in stabilizing a variety of o/w Pickering emulsions[39] and their polymerization proved to be a pathway toward generating a variety of functional hybrid materials, such as molecular imprinted microspheres for removal of pollutants from water,[40] microcapsules for encapsulation of volatiles[41] and colloidosomes for drug-delivery applications.[42] On the other hand the polymerization of inverse w/o Pickering emulsions has also received significant attention, for manufacturing stable macroporous materials and potential application in tissue engineering[43] of polymerized high internal phase emulsions (HIPE),[44] here referred to as polymeric hollow structures. One advantage is that the polymerized HIPE materials obtained from Pickering emulsions have an increased stability as compared to those obtained from surfactants due to reinforced wall structure by particles.[45] The particles bearing a functionality can also impart an additional property to the polymeric hollow structure, such as magnetic[46] or conductive.[47] The main challenge is that in order to obtain the desired emulsion type, either the capping agent/stabilizer of the emulsifying HNP must be changed to tune its affinity to oil or addition of surfactants might be needed.[46] However, the complex system of HNP, oil, water, surfactants and capping agents can be often difficult to control. JNPs could be a viable solution to this problem considering that they can generate stable colloids in water (*via* electrostatic stabilization of one lobe) yet possess a second lobe that is hydrophobic enough to confer a good affinity towards non-polar oils. In this context we have employed the surfactant-free homologous series of JNPs in Pickering emulsion polymerization of Sty and MMA monomers. We were able to polymerize both o/w and w/o Pickering emulsion types that we presented in the functional composition maps in Figure 2. Surface nanostructured PS microbeads or colloidosomes could be obtained for the Sty monomer from 4 mL 3-TSPM JNPs and for an oil: water ratio of 3: 6 (o/w emulsion) with the corresponding SEM images being given in Figure 5. The JNPs used to stabilize the o/w emulsion remain trapped at the interface after polymerization. In Figure 5 B and C it can be clearly seen that the JNPs remain compactly packed in the monolayer at the surface of the polystyrene spheres. The high-resolution SEM image in Figure 5C suggests that JNPs do not appear to possess a preferred orientation at the interface, in agreement with our previous findings on similarly synthesized JNPs at the surface of wax colloidosomes, which could be attributed to the weak polarity contrast between the Janus lobes.[18] Furthermore, these JNPs could only be partially detached from the surface by ultrasonication of the polymer colloidosomes suspended in water with a ½ inch sonotrode and an amplitude of 70% for 10 s and the impressions left by the JNPs on the polystyrene surface can be clearly seen in Figure 5D.

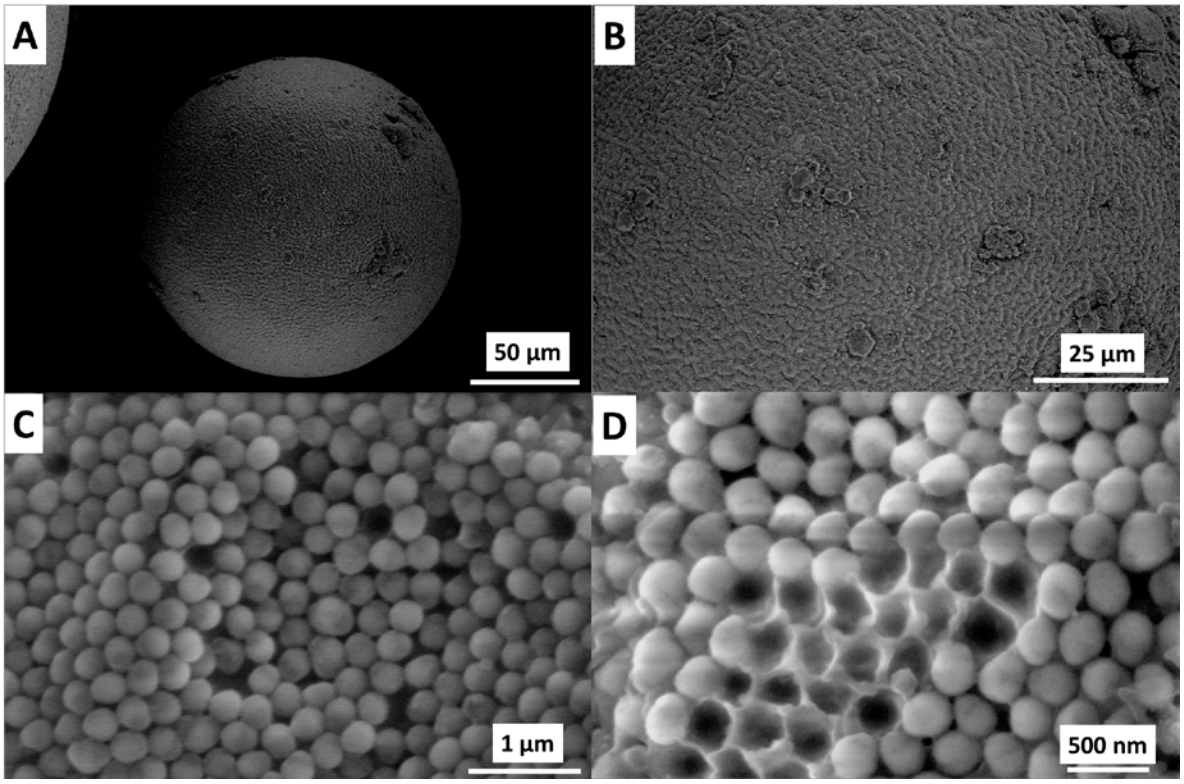

Figure 5. (A) Polystyrene/JNP colloidosomes resulting from the polymerization of a styrene-in-water emulsion obtained from 4 mL 3-TSPM JNPs for ϕ_o = 0.33, see Figure 1. (B) and (C) Polystyrene/JNP colloidosome shows the presence of Janus particle monolayers in which particles appear compactly packed without preferential orientation. (D) Remaining impression from colloidosome in C after JNPs are partially detached from the surface by ultrasonication.

On the other hand, blocks of polystyrene with micro-hollow structure were obtained for smaller lobe size JNPs with a higher affinity for styrene, *e.g.* 2 mL 3-TSPM JNPs for oil: water = 4: 5; see Figure 6 from a w/o emulsion. As before, the JNPs were found at the interface after polymerization but without preferential orientation as observed for higher polarity contrast JNPs.[18] In the hollow structure of the polystyrene block, the emulsified water remains trapped inside and could be partially released by microwaving or heating. The amount of water stored in 1.8 g of polymerized composite can be estimated from the emulsion ratio to be 0.8 mL, which appears to be rather high. Upon 30 min. microwaving, the amount of water that could be released from a 2.3 g sample was 0.6 mL corresponding to 26% of the total weight. Similar polymerization has been carried for MMA as monomer for MMA: water = 5: 4, (2 mL 3-TSPM) JNPs that have a higher affinity for the oil, see Figure S9.

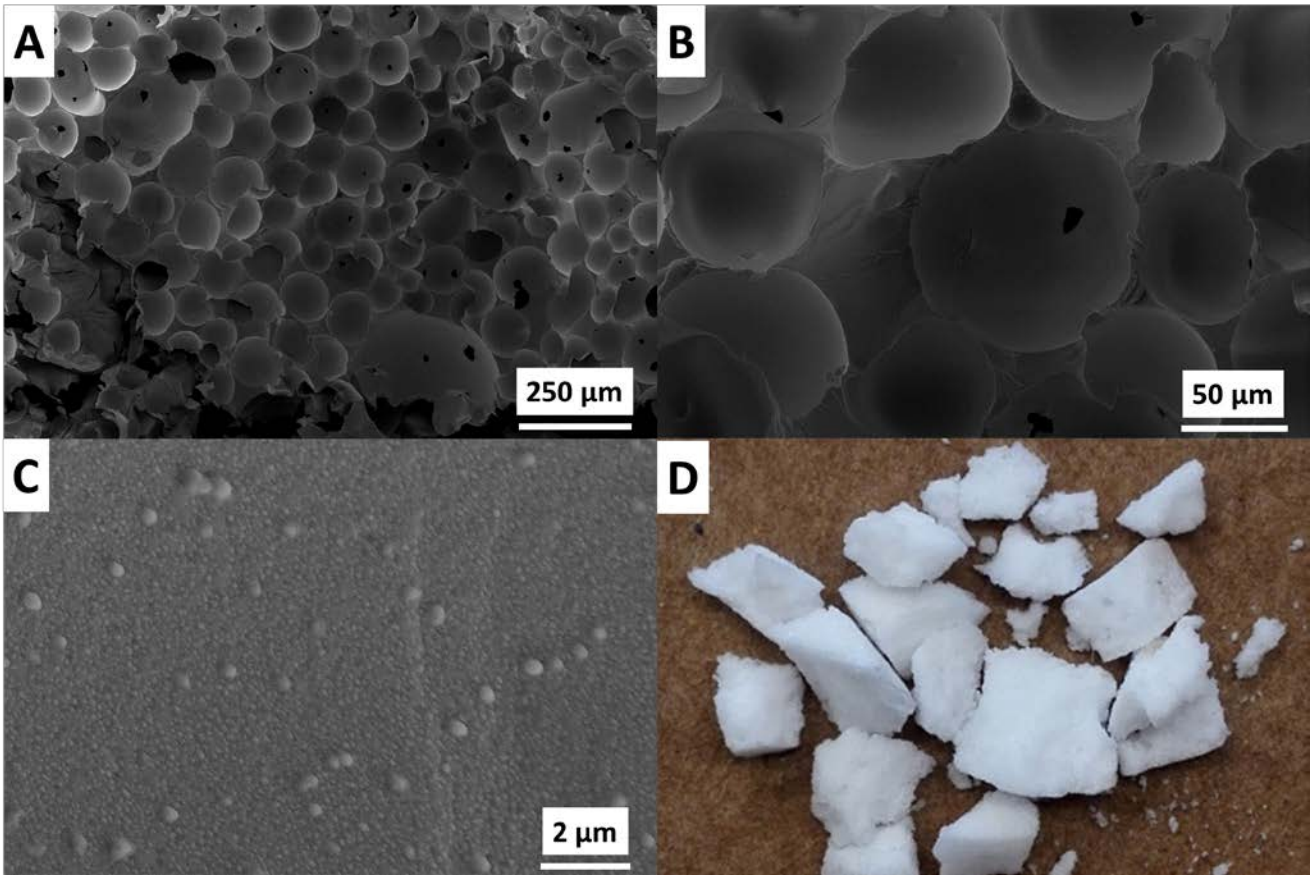

Figure 6. (A) and (B) Cross-section SEM images of the polystyrene/JNP hollow structure resulting from polymerization of a water-in-styrene emulsion obtained from the 2 mL 3-TSPM JNPs for ϕ_o = 0.44, see Figure 1 and Figure 2. (C) The hollow structure has a nanostructured interface due to the presence of the JNPs. The orientation of the particles could not be resolved in this case. (D) Photo' of solidified w/o Pickering emulsion after polymerization.

4. CONCLUSIONS

We have shown that a homologous series of surfactant-free JNPs can be successfully employed in the emulsification of various oils. Transitional and catastrophic phase inversion can be induced. Furthermore, the phase inversion boundary delineating w/o from o/w emulsions depends both on the polarity of the oil and significantly on the polarity of the JNPs varied by an increase in the polar P(3-TSPM) lobe size. The qualitative observations captured in the functional composition maps were than translated into quantitative calculations of JNP/oil interfacial energies by proposing a simple model. The model was based on the assumption that at the emulsion phase inversion boundary the probabilities of formation of o/w and w/o emulsions are equal, therefore the work of adhesion of the oil to JNPs can be related to that of water to JNPs *via* the parameter *f*. The ratio *f* of oil:water at which this occurs was used to gauge the magnitude of the relative strength between the work of adhesion JNP/oil and JNP/water that is responsible for curving the surface toward oil or water. Most importantly

our model shows that it is possible to extract quantitative information about the polarity of particles and could be applied universally to determine relative interfacial energies of any particles with a variety of solvents from w/o to o/w emulsification phase inversion data. While the model proposed here it is currently the only simple and alternative model to estimate the relative interfacial energies of nanoparticles outside the set of existing set of theories that all require the *a priori* measurement of contact angles, it has its limitations, as discussed in *Section 3.3.* In addition this series of JNPs, due to their broad span in surface polarity and HLB, can be used as standard scale or reference by researchers trying to establish interfacial energy and surface polarity of unknown particles by employing same emulsification procedures and compare own results relative to those obtained here.

Finally, we have shown that each type of JNPs-stabilized Pickering emulsion can be polymerized in the absence of surfactant or capping agent. In Pickering emulsification the JNPs bring a clear advantage over HNPs in that the overall polarity and affinity to one of the phase can be tuned gradually and predictably without using capping agents or further surface modifications that is often difficult to control. We obtained surface structured polymeric materials, such as surface nanostructured polymer beads or hollow polymeric materials which retain the aqueous solution inside the closed pores. This could find potential use in long term storage applications.

ASSOCIATED CONTENT

Supporting Information

The Supporting Information is available free of charge on the ACS Publications Website.

Tables summarizing particle diameters, lobe size, HLB balance of JNPs and solvent properties, such as Hansen parameters and surface tension. Figures depicting emulsification results for different solvents and water with JNPs. SEM images showing the hollow structures after polymerization of the MMA monomer Pickering emulsions.

AUTHOR INFORMATION

Corresponding Author: *andrei.honciuc@zhaw.ch, Tel.: +41(0)589345283

ORCID

Andrei Honciuc: 0000-0003-2160-2484;

ACNKOWLEDGEMENTS

We gratefully acknowledge the financial funding from Metrohm Foundation (Herisau) and H2020-SPIRE-2015 (IbD® - Intensified by Design. GA – 680565). We thank the reviewers for the constructive comments.

REFERENCES

(1) Lazghab, M.; Saleh, K.; Pezron, I.; Guigon, P.; Komunjer, L. Wettability Assessment of Finely Divided Solids. *Powder Technol.* **2005**, *157*, 79–91.
(2) Hua, X.; Bevan, M. A.; Frechette, J. Reversible Partitioning of Nanoparticles at an Oil–Water Interface. *Langmuir* **2016**, *32*, 11341–11352.
(3) Zhang, Y.; Wang, S.; Zhou, J.; Zhao, R.; Benz, G.; Tcheimou, S.; Meredith, J. C.; Behrens, S. H. Interfacial Activity of Nonamphiphilic Particles in Fluid–Fluid Interfaces. *Langmuir* **2017**, *33*, 4511–4519.
(4) Tu, F.; Park, B. J.; Lee, D. Thermodynamically Stable Emulsions Using Janus Dumbbells as Colloid Surfactants. *Langmuir* **2013**, *29*, 12679–12687.
(5) Lin, Y.; Skaff, H.; Emrick, T.; Dinsmore, A. D.; Russell, T. P. Nanoparticle Assembly and Transport at Liquid-Liquid Interfaces. *Science* **2003**, *299*, 226–229.
(6) Chibowski, E.; Perea-Carpio, R. Problems of Contact Angle and Solid Surface Free Energy Determination. *Adv. Colloid Interface Sci.* **2002**, *98*, 245–264.
(7) Van Oss, C. J.; Chaudhury, M. K.; Good, R. J. Interfacial Lifshitz-van Der Waals and Polar Interactions in Macroscopic Systems. *Chem. Rev.* **1988**, *88*, 927–941.
(8) Girifalco, L. A.; Good, J. A Theory for Estimation of Surface and Interfacial Energies. *J. Phys. Chem.* **1957**, *61*, 904–909.
(9) Fowkes, F. M. Attractive Forces at Interfaces. *Ind. Eng. Chem.* **1964**, *56*, 40–52.
(10) Good, R. J. Contact Angle, Wetting, and Adhesion: A Critical Review. *Contact Angle Wettability Adhes.* **1993**, 3–36.
(11) Owens, D. K.; Wendt, R. C. Estimation of the Surface Free Energy of Polymers. *J. Appl. Polym. Sci.* **1969**, *13*, 1741–1747.
(12) Kaelble, D. H. Dispersion-Polar Surface Tension Properties of Organic Solids. *J. Adhes.* **1970**, *2*, 66–81.
(13) Wu, S. Surface and Interfacial Tensions of Polymer Melts. II. Poly(methyl Methacrylate), Poly(n-Butyl Methacrylate), and Polystyrene. *J. Phys. Chem.* **1970**, *74*, 632–638.
(14) Zanini, M.; Isa, L. Particle Contact Angles at Fluid Interfaces: Pushing the Boundary beyond Hard Uniform Spherical Colloids. *J. Phys. Condens. Matter* **2016**, *28*, 313002–313026.
(15) Washburn, E. W. The Dynamics of Capillary Flow. *Phys. Rev.* **1921**, *17*, 273–283.
(16) Alghunaim, A.; Kirdponpattara, S.; Newby, B. Z. Techniques for Determining Contact Angle and Wettability of Powders. *Powder Technol.* **2016**, *287*, 201–215.
(17) Galet, L.; Patry, S.; Dodds, J. Determination of the Wettability of Powders by the Washburn Capillary Rise Method with Bed Preparation by a Centrifugal Packing Technique. *J. Colloid Interface Sci.* **2010**, *346*, 470–475.
(18) Wu, D.; Chew, J. W.; Honciuc, A. Polarity Reversal in Homologous Series of Surfactant-Free Janus Nanoparticles: Toward the Next Generation of Amphiphiles. *Langmuir* **2016**, *32*, 6376–6386.
(19) Aveyard, R. Can Janus Particles Give Thermodynamically Stable Pickering Emulsions? *Soft Matter* **2012**, *8*, 5233–5240.
(20) Tu, F.; Lee, D. Shape-Changing and Amphiphilicity-Reversing Janus Particles with pH-Responsive Surfactant Properties. *J. Am. Chem. Soc.* **2014**, *136*, 9999–10006.
(21) Kumar, A.; Park, B. J.; Tu, F.; Lee, D. Amphiphilic Janus Particles at Fluid Interfaces. *Soft Matter* **2013**, *9*, 6604–6617.

(22) Ruhland, T. M.; Gröschel, A. H.; Ballard, N.; Skelhon, T. S.; Walther, A.; Müller, A. H. E.; Bon, S. A. F. Influence of Janus Particle Shape on Their Interfacial Behavior at Liquid–Liquid Interfaces. *Langmuir* **2013**, *29*, 1388–1394.
(23) Kim, Y. J.; Liu, Y. D.; Choi, H. J.; Park, S.-J. Facile Fabrication of Pickering Emulsion Polymerized Polystyrene/laponite Composite Nanoparticles and Their Electrorheology. *J. Colloid Interface Sci.* **2013**, *394*, 108–114.
(24) Walther, A.; Hoffmann, M.; Müller, A. H. E. Emulsion Polymerization Using Janus Particles as Stabilizers. *Angew. Chem. Int. Ed.* **2008**, *47*, 711–714.
(25) Shen, X.; Xu, C.; Ye, L. Imprinted Polymer Beads Enabling Direct and Selective Molecular Separation in Water. *Soft Matter* **2012**, *8*, 7169–7176.
(26) Jin Ahn, W.; Seung Jung, H.; Jin Choi, H. Pickering Emulsion Polymerized Smart Magnetic Poly(methyl methacrylate)/Fe 2 O 3 Composite Particles and Their Stimulus-Response. *RSC Adv.* **2015**, *5*, 23094–23100.
(27) Skelhon, T. S.; Grossiord, N.; Morgan, A. R.; Bon, S. A. F. Quiescent Water-in-Oil Pickering Emulsions as a Route toward Healthier Fruit Juice Infused Chocolate Confectionary. *J. Mater. Chem.* **2012**, *22*, 19289–19295.
(28) Bollhorst, T.; Rezwan, K.; Maas, M. Colloidal Capsules: Nano- and Microcapsules with Colloidal Particle Shells. *Chem. Soc. Rev.* **2017**, *46*, 2091–2126.
(29) Ikem, V. O.; Menner, A.; Bismarck, A. Tailoring the Mechanical Performance of Highly Permeable Macroporous Polymers Synthesized via Pickering Emulsion Templating. *Soft Matter* **2011**, *7*, 6571–6577.
(30) Griffin, C. W. Calculation of HLB Values of Non-Ionic Surfactants. *J. Soc. Cosmet. Chem.* **1955**, *5*, 249–257.
(31) Pasquali, R. C.; Taurozzi, M. P.; Bregni, C. Some Considerations about the Hydrophilic–lipophilic Balance System. *Int. J. Pharm.* **2008**, *356*, 44–51.
(32) Hansen, C. M. *Hansen Solubility Parameters: A User's Handbook*, 2nd ed.; CRC Press: Boca Raton, Florida, 2007.
(33) Finkle, P.; Draper, H. D.; Hildebrand, J. H. The Theory of Emulsification. *J. Am. Chem. Soc.* **1923**, *45*, 2780–2788.
(34) Wilder D. Bancroft. *Applied Colloid Chemistry*, 1st Edition.; McGraw-Hill Book Co.: New York, 1921.
(35) Binks, B. P.; Lumsdon, S. O. Effects of Oil Type and Aqueous Phase Composition on Oil–water Mixtures Containing Particles of Intermediate Hydrophobicity. *Phys. Chem. Chem. Phys.* **2000**, *2*, 2959–2967.
(36) Israelachvili, J. N. Adhesion and Wetting Phenomena. In *Intermolecular and Surface Forces: Revised*; Academic Press, London, 2011; pp 415–467.
(37) Chern, C. S. Emulsion Polymerization Mechanisms and Kinetics. *Prog. Polym. Sci.* **2006**, *31*, 443–486.
(38) Thickett, S. C.; Gilbert, R. G. Emulsion Polymerization: State of the Art in Kinetics and Mechanisms. *Polymer* **2007**, *48* (24), 6965–6991.
(39) Binks, B. P.; Lumsdon, S. O. Pickering Emulsions Stabilized by Monodisperse Latex Particles: Effects of Particle Size. *Langmuir* **2001**, *17*, 4540–4547.
(40) Fan, T.; Yang, W.; Wang, N.; Ni, X.; Wen, J.; Xu, W. Molecularly Imprinted Polymer Microspheres Derived from Pickering Emulsions Polymerization in Determination of di(2-Ethylhexyl) Phthalate in Bottled Water Samples. *J. Appl. Polym. Sci.* **2016**, *133*, 43484–43495.
(41) Zhang, L.; Zhang, Y.; Xu, H.; Wang, H.; Du, Q. Polymer/graphene Oxide Composite Microcapsules with Greatly Improved Barrier Properties. *RSC Adv* **2016**, *6*, 7618–7625.
(42) Wu, J.; Ma, G.-H. Recent Studies of Pickering Emulsions: Particles Make the Difference. *Small* **2016**, *12*, 4633–4648.
(43) Liu, X.; Okada, M.; Maeda, H.; Fujii, S.; Furuzono, T. Hydroxyapatite/biodegradable Poly(l-Lactide–co-E-Caprolactone) Composite Microparticles as Injectable Scaffolds by a Pickering Emulsion Route. *Acta Biomater.* **2011**, *7*, 821–828.
(44) Ikem, V. O.; Menner, A.; Horozov, T. S.; Bismarck, A. Highly Permeable Macroporous Polymers Synthesized from Pickering Medium and High Internal Phase Emulsion Templates. *Adv. Mater.* **2010**, *22*, 3588–3592.

(45) Ikem, V. O.; Menner, A.; Bismarck, A. Tailoring the Mechanical Performance of Highly Permeable Macroporous Polymers Synthesized via Pickering Emulsion Templating. *Soft Matter* **2011**, *7*, 6571–6577.
(46) Vílchez, A.; Rodríguez-Abreu, C.; Esquena, J.; Menner, A.; Bismarck, A. Macroporous Polymers Obtained in Highly Concentrated Emulsions Stabilized Solely with Magnetic Nanoparticles. *Langmuir* **2011**, *27*, 13342–13352.
(47) Zhang, W. L.; Park, B. J.; Choi, H. J. Colloidal Graphene Oxide/polyaniline Nanocomposite and Its Electrorheology. *Chem. Commun.* **2010**, *46*, 5596–5598.